Supporting Information:

Preparation of carbon nanotube/inorganic nanoparticle composite films: CNTs with exfoliated $Bi_2Si_2Te_6$ nanosheets for carbon-based thermoelectric generator applications

Dabin Park[a], Minsu Kim[a] and Jooheon Kim[a,b,c]*

[a]School of Chemical Engineering & Materials Science,

Chung-Ang University, Seoul 06974, Republic of Korea

[b]Department of Advance Materials Engineering,

Chung-Ang University, Anseong 17546, Republic of Korea

[c]Department of Intelligent Energy and Industry, Graduate School,

Chung-Ang University, Seoul 06974, Republic of Korea

*Corresponding author: jooheonkim@cau.ac.kr (J. Kim)

Supporting Information Contents:

1. Supplementary Notes

2. Figures

3. Tables

Note 1. Expeimental Methods

1.1. Materials

Bismuth (99%, Bi), powder, silicon (99%, Si), tellurium (99%, Te), Single-walled carbon nanotubes (SWCNTs), and lithium hydroxide (98%, LiOH) were purchased from Sigma-Aldrich (St. Louis, MO). Ethylene glycol (99%, $C_2H_4(OH)_2$), hydrochloric acid (35-37%, HCl), acetone (99.8%, CH_3COCH_3) and ethanol (94.5%, C_2H_5OH) were supplied from Daejung Chemicals & Metals Co. (Seoul, Korea).

1.2. Composite preparation

A $Bi_2Si_2Te_6$ ingot was prepared adopting a solid-state reaction. Briefly, stoichiometric amounts of Bi, Si, and Te were loaded into a quartz ampoule, which was then evacuated, sealed by flame, and slowly heated up to 873 K in 6 h. After keeping this temperature for 24 h, the furnace was subsequently cooled to room temperature (298 K). The prepared ingot was then ground into fine powders with an agate mortar and ball milled using zirconia balls in an inert atmosphere. Subsequently, 1 g of $Bi_2Si_2Te_6$ powder was placed into a Teflon-lined autoclave filled with a solution consisting of 200 ml of ethylene glycol and 0.8 g of LiOH. The autoclave was heated at 473 K for 48 h to achieve the intercalation of the lithium ions into the layered $Bi_2Si_2Te_6$. The solution was then allowed to cool down naturally to room temperature. The resulting product was collected by filtration, rinsed many times with acetone to eliminate the residual reactant, and then dried in a vacuum oven at 333 K for 24 h. Afterwards, 0.5 g of Li-intercalated $Bi_2Si_2Te_6$ powder was placed into a laboratory beaker filled with 200 ml of deionized (DI) water. The beaker was then sealed and sonicated at low power for 1 h. The resulting dispersions were centrifuged at 1000 rpm for 30 min and then the supernatant was collected. Next, the supernatant was centrifuged at 8000 rpm for 30 min. The resulting powder

was purified several times with 3 vol.% HCl and DI water to remove possible oxidized layers from the nanosheet surface. The final BST NSs was collected after repeatedly washing with ethanol, and then dried in a vacuum oven. To prepare the BST/CNT composite, certain amounts of BST NSs and CNTs were dispersed in 10 mL of ethanol. The total weight of the solid materials containing various properties of MWCNTs was controlled to 0.01 g. The resulting solution was ultrasonicated for 30 min. After ultrasonication, the composite filtered through a nylon membrane filter paper to obtain the composite samples, which were dried at 333 K for 12 h and then hot-pressed at 333 K for 1 h.

1.3. Device preparation.

The composite films were cut into strips (18 × 6 mm) and pasted onto a polyimide film at ~6 mm intervals. The copper wires were used to connect the legs, and silver (Ag) adhesives were used to join the ends of the strips. Finally, the TE prototype was encapsulated by a transparent tape to test the output performance. A multimeter (SENIT, A830L) and thermocouple were used to measure the electric properties and temperature differences.

1.4. Characterization

X-ray diffraction (XRD, New D8 Advance, Bruker AXS) was used to characterize the crystal structures of the synthesized materials. XRD was performed at 40 mA, 40 kV, and a scan rate of 1°/s, with 2θ ranging from 5° to 70° using Cu Kα radiation (λ = 0.154056 nm). The binding energy peaks of the synthesized materials were investigated with X-ray photoelectron spectroscopy (XPS, VG-Microtech, ESCA2000). The microstructure was observed with field-emission scanning electron spectroscopy (FE-SEM, SIGMA), field-emission transmission microscopy (FE-TEM, JEM-2100F), and Cs-corrected scanning transmission microscopy (Cs-STEM, JEM-ARM200F, JEOL Ltd). Elemental mappings of the samples were analyzed by

energy-dispersive X-ray spectroscopy (EDS, NORAN system 7, Thermo Scientific).

The charge carrier concentration (n) and mobility (μ) were measured using Hall-effect measurements (HMS-300, Ecopia). The electrical conductivity and Seebeck coefficient were investigated using an Ulvac Riko ZEM-3 instrument under a helium atmosphere. All thermoelectric properties of samples were measured with in-plane. Five replicates of the composite samples were used for each test to verify the reproducibility of the experiments.

Note 2. The power density of the TE device

When ignoring the contact resistance and electrode resistance of the TE device, the power density is inferred by the following equation:

$$P_{density} = \frac{P_{max}}{N \cdot A} = \frac{(N \cdot S \cdot \Delta T)^2 / 4 \cdot N \cdot \frac{l}{\sigma \cdot w \cdot t}}{N \cdot w \cdot t} = \frac{S^2 \cdot \sigma}{4l} \cdot \Delta T^2 \quad (2)$$

whrer N is the number of TE legs, A, S, σ, w, l and t are the area, Seebeck coefficient, electrical conductivity, width, length and thickness of a each strip, respectibly. Therefore, the power density of the TE device is related to the Seebeck coefficient, electrcal conductivity, and the length of the TE legs, and the temperature difference that can indirectly determined the TE performance of the materials.

2. Figures

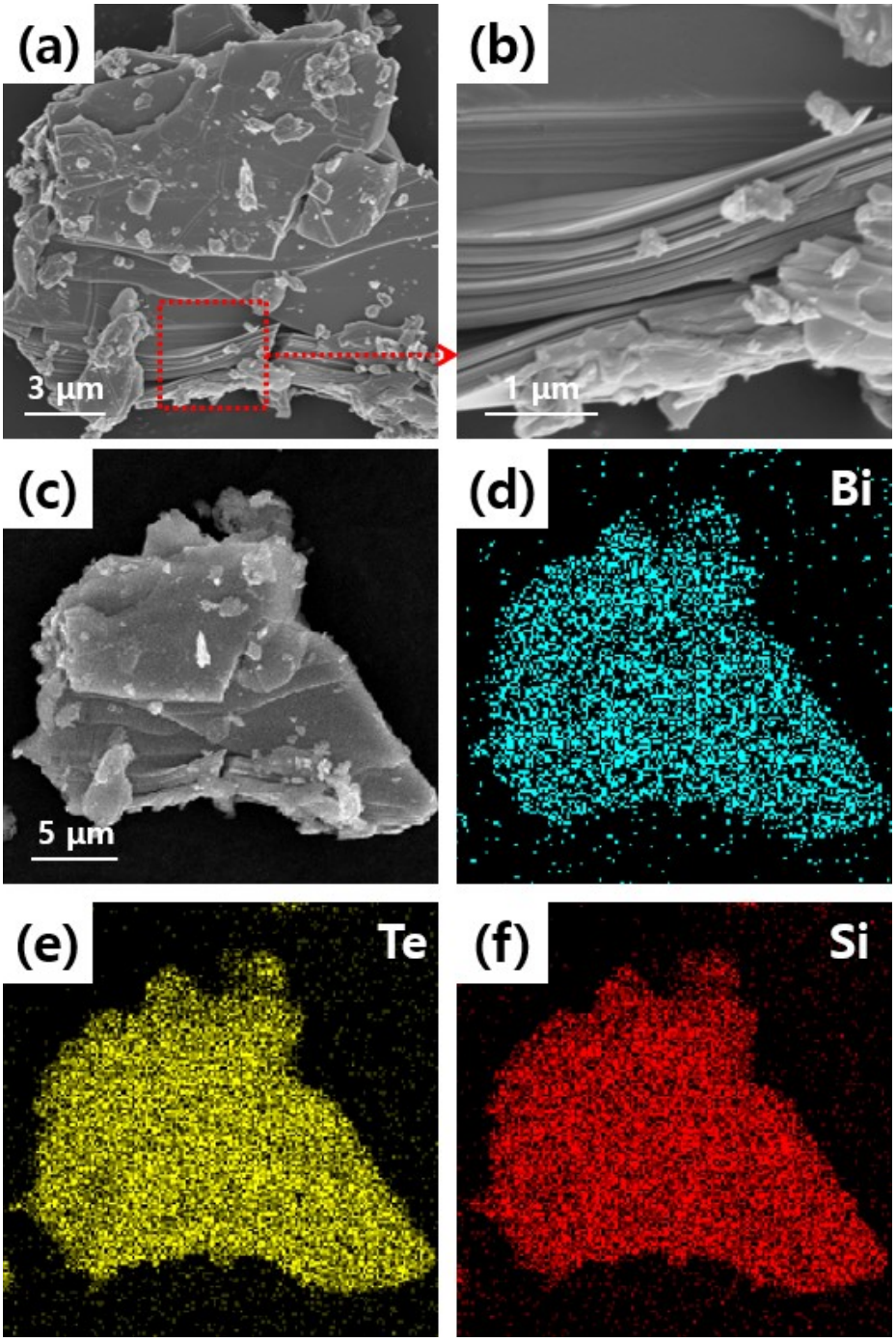

Fig.. S1. (a) low- and (b) high-magnification FE-SEM images of BST ingot. FE-SEM image and the corresponding EDS mapping images of (c) BST ingot (d-f) corresponding EDS mapping images of $Bi_2Si_2Te_6$ ingot.

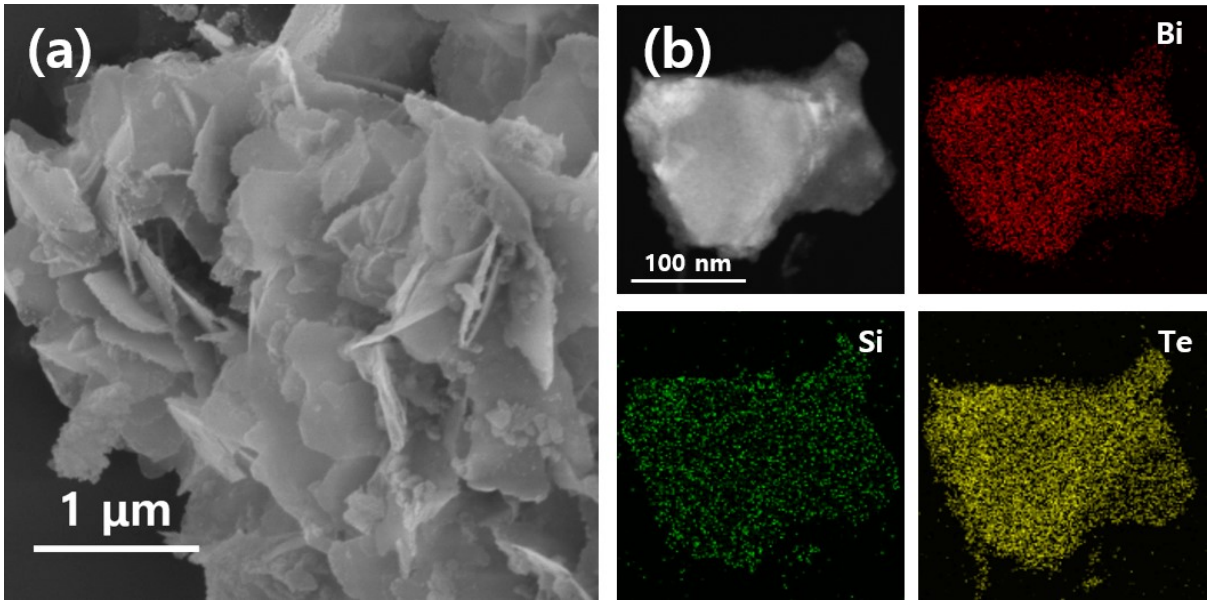

Fig. S2. (a) FE-SEM and (b) TEM-EDS atomic mapping of BST NS.

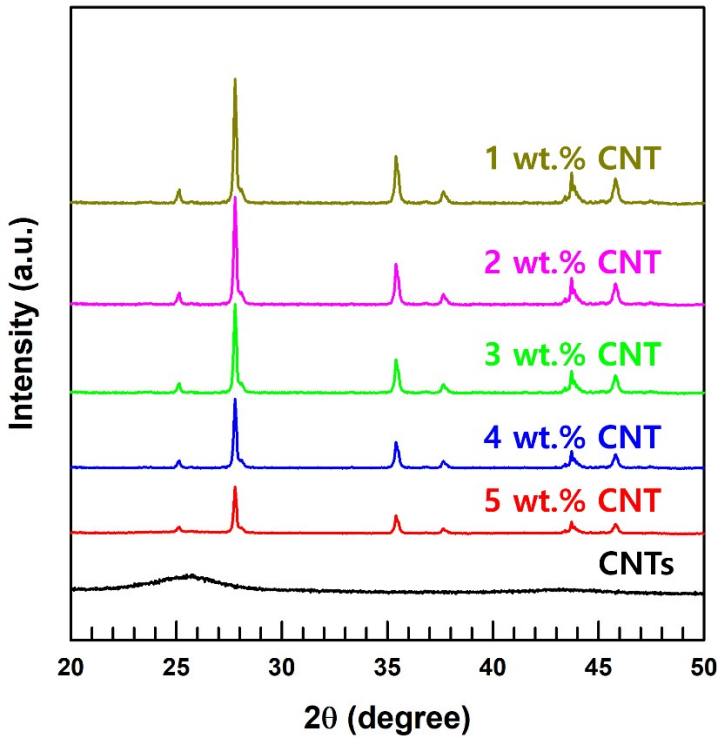

Fig. S3. (a) XRD pattern of CNT and BST NS/CNT composite with various CNT contents.

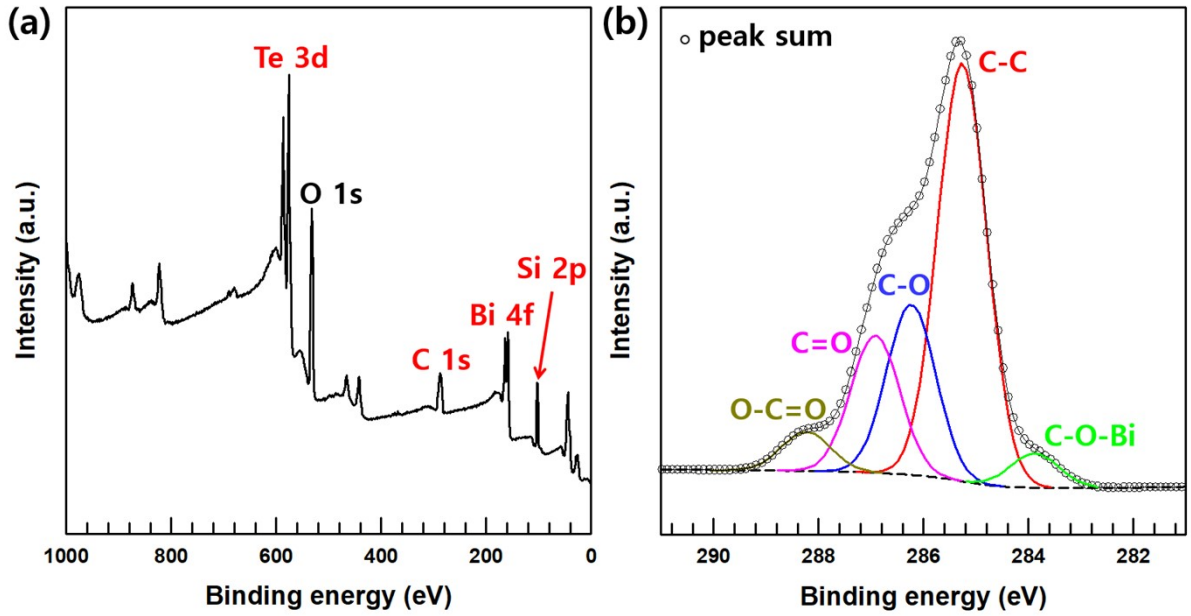

Fig. S4. (a) XPS wide scan and (b) C 1s region of BST/CNT composite with 3 wt.% CNT.

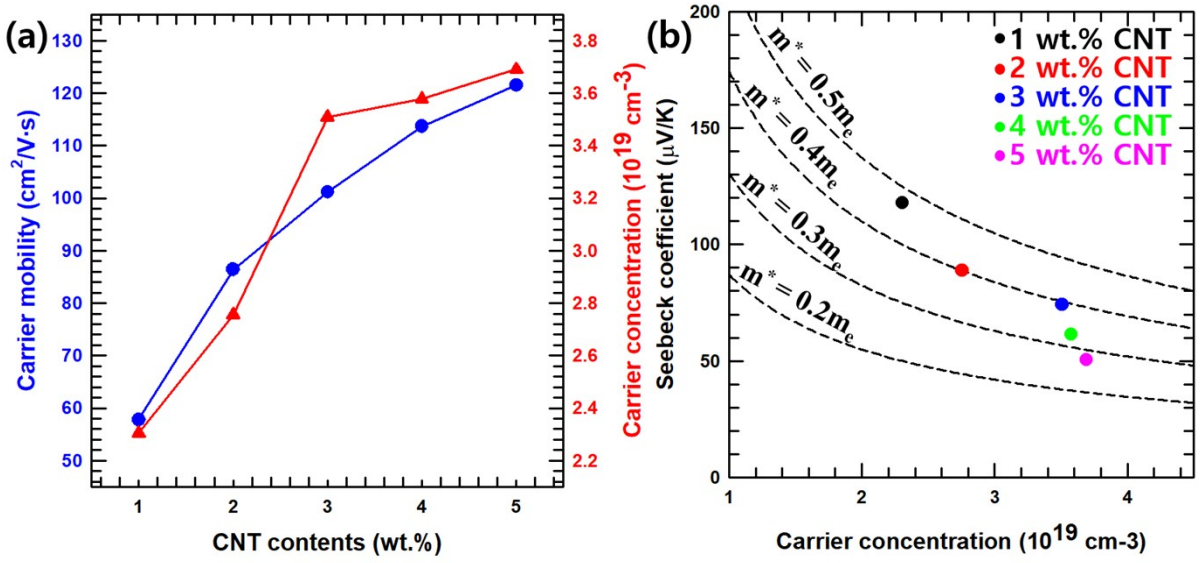

Fig. S5. (a) Carrier concentration and mobility values of BST/CNT composite with different CNT contents. (b) Seebeck coefficiet *S versus* carrier concentration of the BST/CNT composites. Dashed line are the calurated Pisarenko plot for various effective mass as indicated.

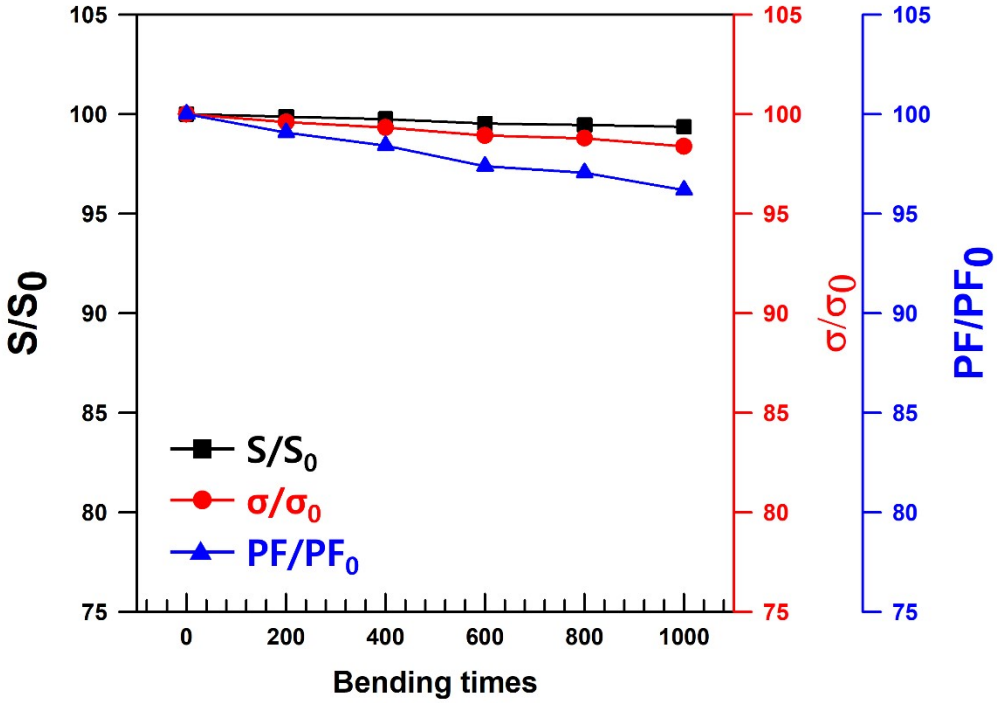

Fig. S6. Demonstration of ratio of Seebeck coefficient (S/S_0), electrical conductivity (σ/σ_0), ann power factor (PF/PF_0) as a function of bending cycles.

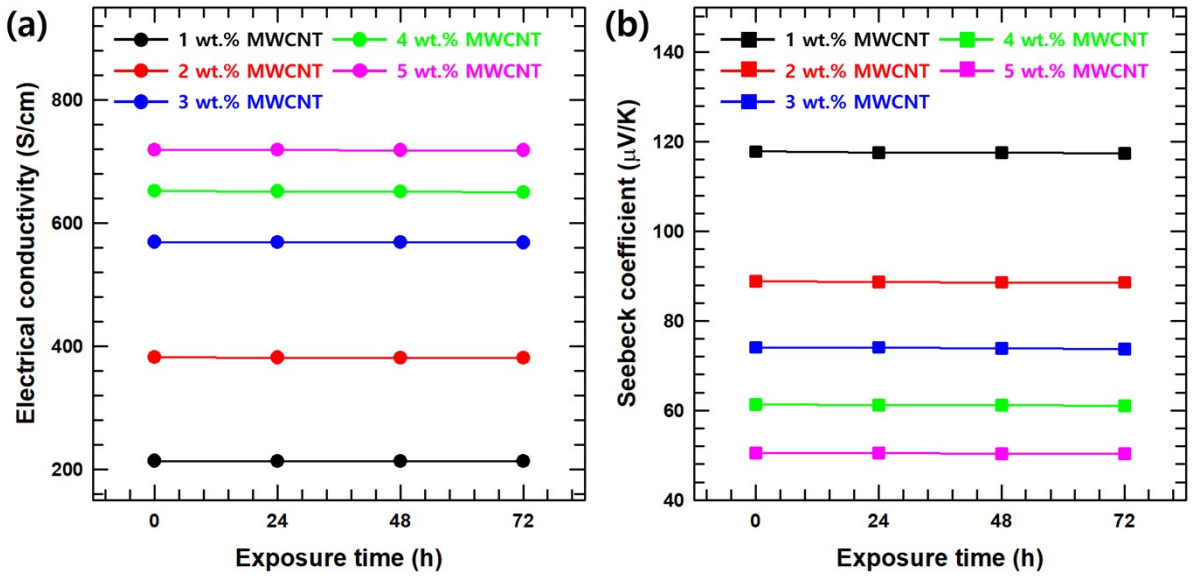

Fig. S7. The stability in air shown in (a) electrical conductivity and (b) Seebeck coefficient values after exposure for different times.

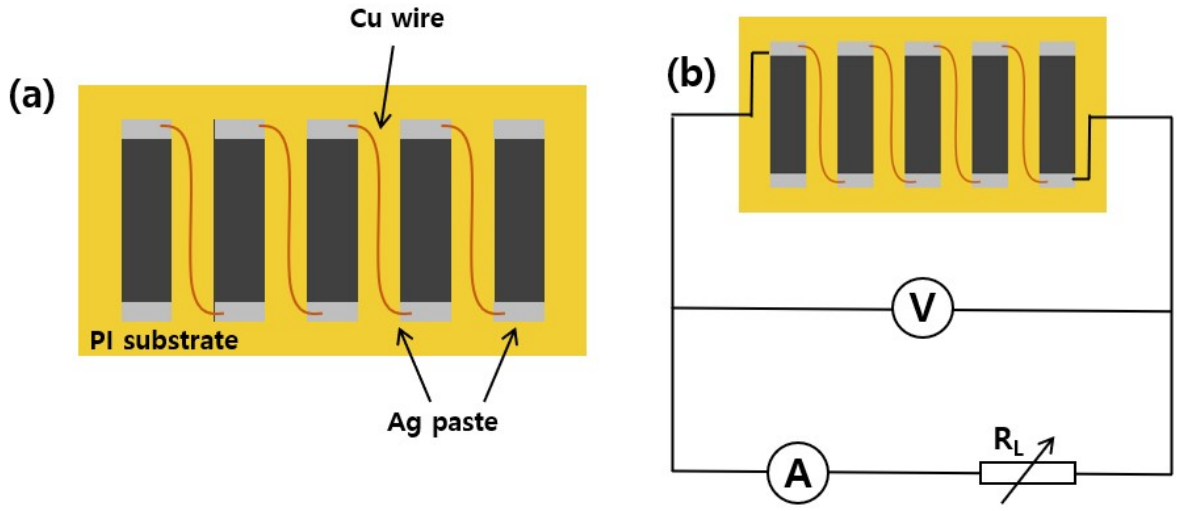

Fig. S8. Schematic diagram of the (a) TE generator and (b) electrical circuit for the performance measurement of TE generator.

3. Tables

	σ (S/cm)	S (μV/K)	PF (μW/m·K^2)	*Ref.*
SWCNTs	~650 - 1100	~15.5 - 19	~23.5 – 26.4	1
$Bi_2Si_2Te_6$ NSs	~116.7	~129.8	~193.9	This study
$Bi_2Si_2Te_6$	~120	~125	~187.5	2
$Bi_2Si_2Te_6$	~80	~160	~204.8	3
BST NS/CNT composite with 1 wt.% of CNTs	~213.4	~117.8	~296.1	This study
BST NS/CNT composite with 2 wt.% of CNTs	~381.4	~88.9	~301.4	This study
BST NS/CNT composite with 3 wt.% of CNTs	~568.9	~74.1	~312.4	This study
BST NS/CNT composite with 4 wt.% of CNTs	~651.7	~61.3	~244.9	This study
BST NS/CNT composite with 4 wt.% of CNTs	~718.4	~50.5	~183.2	This study

Table S1. Thermoelectric properties (σ, S, PF) of BST NSs, SWCNT, and BST/CNT composites with various CNT contents

Materials	Power factor ($S^2 \cdot \sigma$) ($\mu W/(m \cdot K^2)$)	Temperature (K)	References
Bi_2Te_3/CNT fabric	~0.15	Room temperature	4
SWCNT-SnSe	~58.86	Room temperature	5
MWCNT/SnSe/PEDOT:PSS	~59.35	~380	6
Bi_2S_3-MWCNT	~120	~575	7
Bi_2S_3/f-MWCNT	~151	~575	8
Bi_2Te_3-CNT	~210	~480	9
SWCNT/PANI	~362	Room temperature	10
$Bi_2Si_2Te_6$ NS/CNT	~498.3	~423	

Table S2. Power factor values of CNT based thermoelectric composite materials compared with previously reported materials.

Composites	Power density (W/m^2)	ref
PEDOT:PSS-SWCNT /C_{60}-TiS_2	1.68	11
Ag_2Se/Nylon membrane	2.3	12
PANI-Ag_2Se/PVDF	2.33	13
BST NS/CNT	~10.7	This study

Table S3. Power density of BST NS/CNT composite films compared with previously reported flexible thermoelectric materials.

References

1. W. Zhou, J. Vavro, N. M. Nemes, J. E. Fischer, F. Borondics, K. Kamaras, D. B. Tanner, *Phys. Rev. B*, **2005**, *71*, 205423
2. Y. Luo, Z. Ma, S. Hao, S. Cai, Z.-Z. Luo, C. Wolverton, V. P. Dravid, J. Yang, Q. Yan and M. G. Kanatzidis, *J. Am. Chem. Soc.*, 2022, **144**, 1445-1454.
3. C. Chen, D. Shen, C. Xia, Z. Zhang, W. Wang, Q. Zhang and Y. Chen, *Chem. Eng. J.*, 2022, **441**, 135968.
4. D. Ding, Q. Wu, J. Wang, Y. Chen, Q. Li, L. Hou, L. Zhao, Y-Y. Xu, *Compos. Commun.*, 2023, **38**, 101509.
5. J. Fan, X. Wang, F. Liu, Z. Chen, G. Chen, *ACS Appl. Mater. Interfaces*, 2021, **13**, 30731-30738.
6. D. Liu, Z. Yan, Y. Zhao, Z. Zhang, Y. Zheng, B. Zhang, P. Shi, C. Xue, *J. Alloys. Compd.*, 2022, **898**, 162844.
7. Y. Liao, W. Liu, W. Jia, B. Wang, L. Chen, K. Huang, M. J. Montgomery, J. Qian, S. Lv, L. D. Pfefferle, *Adv. Electron. Mater.*, 2021, **7**, 2100468.
8. Y. Bai, X. Li, T. Ouyang, W. Wang, Y. Yan, X. Jiang, X. Wang, Z. Wang, X. Cai, J. Cai, Z. Ge, H. Tan, *Carbon*, 2023, **212**, 118158.
9. Y. Zhao, Y. Li, J. Qiao, S. Jiang, P. Mao, J. Qiu, S. Kang, J. Tan, K. Tai, C. Liu, *Carbon*, 2020, **170**, 191-198.
10. P. Li, Y. Zhao, H. Li, S. Liu, Y. Liang, X. Cheng, C. He, *Compos. Sci. Technol.*, 2020, **189**, 108023.
11. L. Wang, Z. Zhang, L. Geng, T. Yuan, Y. Liu, J. Guo, L. Fang, J. Qui, S. Wang, *Energy Environ. Sci*., **2018**, *11*, 1307-1317.
12. Y. Ding, Y. Qui, K. Cai, Q. Yao, S. Chen, L. Chen, J. He, *Nat. Commun*., **2019**, *10*, 841.

13. D. Park, M. Kim, J. Kim, *J. Alloys. Compd*., **2021**, *884*, 161098.